Bound Solitons Induced by Noise-Mediated Casimir-Like Interactions

Kfir Sulimany[1,*], Offek Tziperman[1,*], Yaron Bromberg[1], and Omri Gat [1,2]

[1]Racah Institute of Physics, The Hebrew University of Jerusalem, Jerusalem 91904, Israel
[*]Co-first authors with equal contribution
[2]Corresponding author: omrigat@mail.huji.ac.il

Abstract

We study experimentally and theoretically the steady states of optical solitons that aggregate into bunches in a fiber laser. The laser is passively mode-locked by a nonlinear multimode interference based saturable absorber. By modifying the laser gain via its pumping current, we demonstrate a variety of steady states. We model the steady states using our recently proposed noise-mediated Casimir-like pulse interaction mechanism and obtain a quantitative agreement with our experimental results. We present a steady state phase diagram and demonstrate transitions between noise-mediated incoherent bound states and coherently coupled bound states without using additional modulators, asserting the noise-mediated interaction as a dominant mechanism in such complex soliton structures.

1 Introduction

Dissipative solitons are localized waves in open systems far from equilibrium, whose existence result from a balance of dissipative and dispersive effects. They appear in numerous physical areas including reaction-diffusion systems, neurological and ecological sciences, fluid dynamics, and photonics [1–7]. Photonics is a great platform to observe the nonlinear complex behavior of dissipative solitons [8–14]. In particular, collective nonlinear phenomena such as the aggregation of solitons into bunches have created great interest [15, 15–28].

Multi-soliton patterns exhibit an extensive pallet of short and long-range pulse interactions. Short-range interactions take place when pulse tails overlap [21, 29–32]. However, interactions over separations of orders of magnitude beyond the width of individual solitons must be mediated by the the gain [19, 33], or by acoustic response [17, 34, 35]. Furthermore, non-soliton components of optical pulses, such as dispersive-wave pedestals give rise to interactions with an intermediate range significantly longer than the soliton width, but much shorter than the cavity length [18, 36]. Recently, the transition between complex soliton states has been achieved utilizing optical modulation components [35, 37, 38]. However, a model that captures the dynamics of both coherently coupled and incoherently coupled solitons is still lacking.

Recently, we introduced a long-range interaction mechanism arising from the effect of gain depletion in the presence of noisy quasi-CW light in a mode-locked laser [33, 39]. The interaction results from the reduction of optical fluctuations due to gain depletion, following the passage of a pulse through the gain medium. Suppression of fluctuations decrease the temporal jitter of subsequent pulses and in this way bias the jitter and sets the pulse motion. This noise-mediated interaction (NMI) mechanism shares some intriguing properties with the Casimir effect in quantum electrodynamics, where macroscopic objects experience an effective interaction due to suppression of electromagnetic field fluctuations [40]. In both the NMI and the Casimir effect, distant objects inhibit microscopic fluctuations in extended electromagnetic modes. The consequent breaking of spatiotemporal homogeneity gives rise to the weak interactions among these objects.

Optical solitons in anomalous-dispersion mode-locked lasers are often accompanied by weak and broad dispaerswave pedestals [41]. When solitons are well-separated, the NMI is generally attractive [33], but when two solitons are close enough that their pedestals overlap, the interaction can become repulsive; consequently NMI can lead to the formation of bound states of solitons whose steady-state separation is comparable with the pedestal width. The overall phases of solitons in such bound states are not coherently locked, so that they can be viewed as *loosely bound*.

The propagation of dispersive waves in a mode-locked laser is highly sensitive to the overall net gain, which means that the pedestals can be controlled by the amplifier pump. Here, we use this control knob to experimentally observe and manipulate the steady state of a two-pulse waveform in an all-fiber laser that is passively mode-locked. Satuable absorption is achieved by a nonlinear multimode interference [42]. The NMI theory makes precise predictions about the dependence of the pulse separation on the pedestal power and width, which are in quantitative agreement with the experimental measurements, demonstrating that NMI is the

dominant mechanism in long-range pulse interactions in mode-locked fiber lasers of this type.

Even though, as explained, the pedestal overlap induces effective inter-pulse repulsion, repulsion is strong enough to generate only for a large enough pedestal power. Our experiment confirm this theoretical prediction, and demonstrate a transition to a state with *tightly bound* solitons with locked phases, below the pedestal power threshold. The controllability of the pulse separation and the ability to switch from tightly- and loosely-bound soliton regime, constitute a significant step toward applications of multipulse laser waveforms.

2 Results

2.1 Mode-Locked Fiber Laser

The mode-loked laser is based on an all-fiber integrated ring cavity operated in the anomalous dispersion regime [43]. The cavity length is 14m, including a 2.7m erbium-doped fiber gain medium, as depicted in Figure 1. The erbium-doped fiber is core pumped by a 976 nm diode laser through a wavelength-division multiplexer. A polarization-independent optical isolator ensures unidirectional lasing and two fiber polarization controllers tune the overall low cavity birefringence. Finally, a 90/10 coupler provides the laser output.

The mode-locking operation is passively achieved by employing a nonlinear multimode interference-based saturable absorber [44–51]. In this scheme, light occupying a single spatial mode is coupled to a multimode fiber (MMF), whose output facet is spliced to a single mode fiber as depicted in Figure 1. The intensity at the splicing point depends on the interference of the excited MMF modes. At high power, the interference is modified by Kerr nonlinearity making the transmittance at the splicing point power-dependent. In our setup, we utilize a 1.5 m long segment of graded-index multimode fiber (OM1; 62.5 μm core diameter, NA = 0.22) adopted as an effective saturable absorber. This design allows us to modify the absorber properties, such as linear loss, saturated loss, and saturation power, by adjusting the MMF position and the polarization controller. As a result, a wider range of soliton configurations can be achieved [52]. The laser output were analyzed at the laser output with an optical spectrum analyzer (Yokagawa AQ6374), and a fast photodiode connected to a real-time oscilloscope (Tektronix MSO70804C).

We produce stationary patterns of soliton pairs by varying the pump power beyond the threshold for stable single-pulse operation. The laser output spectrum is presented Figure 2(a) as a function of the pumping current . The central wavelength is 1561 nm, and the full width at half maximum bandwidth is ∼3.8 nm. At pump currents below 120 mA ??, we observe spectral fringes indicating that the solitons interact coherently, so that their phases

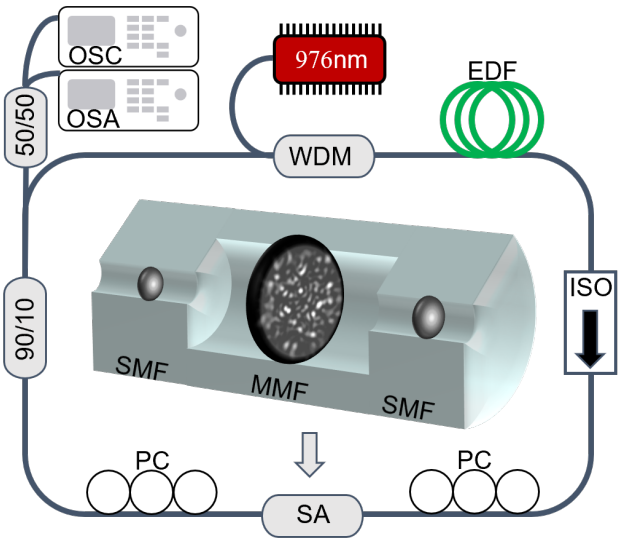

Figure 1: SA: saturable absorber, SMF: single mode fiber, MMF: multimode fiber, EDF: erbium-doped fiber, WDM: wavelength-division multiplexer, ISO: optical isolator, PC: polarization controller, OSA: optical spectrum analyzer, OSC: oscilloscope.

are locked, i.e the solitons tightly bound; at higher pumping currents there are no interference fringes, so that the pulse phases are not coherently locked, which means that the solitons are loosely bound.

Narrow sidebands appear at the primary Gordon-Kelly resonances [53, 54], 1553 nm and 1567 nm, and their power grows with the pumping current. Figure 2(c) presents two spectral cross-sections of Figure 2(a), at pumping currents of 123 mA (blue) and 120 mA (red), exhibiting the Kelly sidebands and the interference fringes in the latter.

Figure 2(b) presents time domain traces of the cavity waveform intensity as a function of the pumping current, where two maxima are observed at high enough pump currents, above 121 mA. At lower pump currents the soliton separation is too small to be resolved in the oscilloscope, but the approximate conservation of total energy in the soliton waveform shows that the number of solitons has not changed. Indeed, the time-domain cross sections at pumping currents of 123 mA (blue) and 120 mA (red) presented in Figure 2(d), imply that both waveforms have equal total energy, proportional to the total area under the curves, as expected from the clamping of the soliton energy in anomalous-dispersion passively mode-locked lasers [55–57]. At 120 mA in particular, the separation time is estimated from the spectral interference pattern at a few ps, far below the electronic resolution of the 8 GHz bandwidth of the oscilloscope.

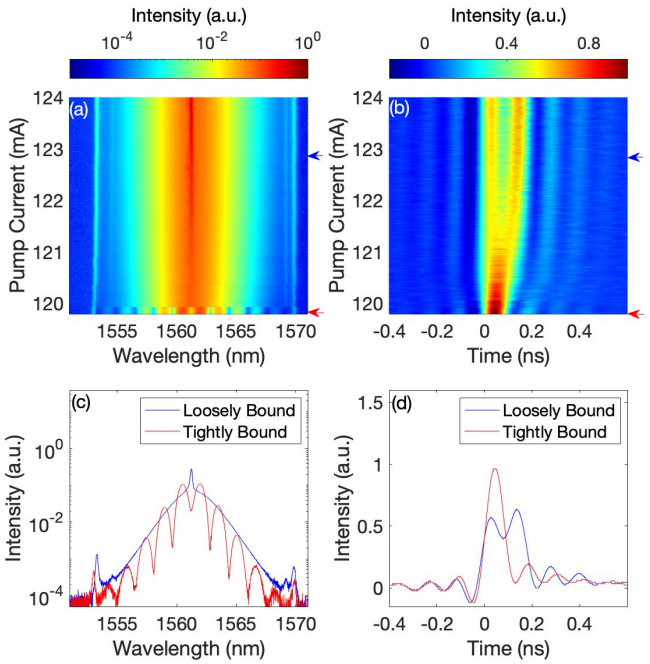

Figure 2: (a) The laser's output spectrum measured as a function of the pumping current. Cross sections at pumping powers of 123 mA (blue arrow) and 120 mA (red arrows) are plotted in (d) demonstrate the two soliton binding regimes; Loosely bound (LB) pairs with fluctuating relative phase and Tightly bound (TB) pairs with coherently locked phases. (b) The lasers temporal profile measured as a function of the pumping current using a fast photodetcor (d) Cross sections at pumping powers of 123 mA (blue arrow) and 120 mA (red arrows) are plotted in (d) demonstrate that the total energy in the soliton waveform remains nearly constant even when the inter-soliton separation is too small to be resolved by the oscilloscope.

2.2 Noise-Mediated Soliton Interaction

The NMI mechanism was first proposed in [33], together with the basic equations of motion governing the pulse motion. The interaction is based on fluctuations of pulse timing generated by overlap with the quasi-CW permeating the cavity, and is mediated by the gain dynamics, and is therefore expected to work in any multi-pulse mode locked laser, although its importance compared with other interaction mechanism can vary widely between different systems. We briefly explain the principles of NMI in with emphasis on the aspects relevant to the present work, and refer the reader to [33] for more details.

We approximate the the laser waveform form as the sum of n non-overlapping soliton waveforms centered at time points t_n (in the frame moving with the group velocity of a single soliton), each of which is accompanied by a weak and broad dispersive-wave pedestal generated by the Gordon-Kelly resonances [41], and an extended quasi-CW waveform; the quasi-CW is generated by noise buildup, and therefore has random phase, as indicated in Figure 3. The growth of the quasi-CW is limited by the small signal net loss, and therefore the quasi-CW intensity is inversely proportional to the net loss. However, since the amplifier gain is depleted by the passage of a pulse, and gain recovery is slow, the gain profile $g(t)$ is nonuniform, which means that the quasi-CW intensity is not uniform either.

The gain profile is governed by the differential equation

$$\frac{dg}{dt} = \frac{\partial(g_u - g)}{\partial t_{rec}} \tag{1}$$

see figure 3.

The overlap of a pulse and the noisy continuum is a source of timing jitter [58, 59], which can be modeled as diffusion process We begin this section by describing the NMI and calculating its steady states, highlighting the results from [33]. We then discuss cases where no loosely bound steady states exist, in which NMI causes attraction between the pulses for any separation. Considering the regimes where small separation is obtained, we explain the transition from a steady state caused by NMI to a steady state caused by a coherent interaction.

The NMI is a byproduct of the pulse timing jitter caused by nonlinear interaction between the pulses and a weak quasi-CW light that runs in the cavity in addition to the pulses. The instantaneous power of the quasi-CW light is determined by the time dependent gain profile.

We assume that the time-dependent gain profile is depleted by the pulses. In our model, the pulse consists of an incoherent sum of a soliton and a low amplitude pedestal centered around the pulses, caused by Kelly-Gordon resonances [41, 53]. The temporal width of the solitons is much smaller than any other relevant timescale, leading to a sharp drop in the gain profile. The pedestal waveform of the nth pulse, normalized by the pulse energy and governed by the Kelly resonant, is $\tilde{E}_{ped}/(2\tilde{w}t_R)e^{-\frac{|t-t_n|}{\tilde{w}t_R}}$ where $\tilde{E}_{ped}$ and $\tilde{w}$ are the pedestal energy and width normalized by the pulse energy and the cavity round trip time (t_R), respectively. These variables are the only unitless quantities determining the normalized stable separation time. The gain depletion due to the pedestals smoothens the gain profile. We a assume a constant recovery rate of the gain in the medium between pulses (Figure 3).

where g_u is the unsaturated gain and t_{rec} is the recovery time; these parameters are determined by the pumping regime. Given the depletion resulting from the solitons as well as the pedestals, and the linear recovery, a saw-tooth tooth temporal gain profile shape is obtained as seen in Figure 3. Accordingly, the quasi-CW power also exhibits a smoothed saw-tooth profile. The interaction between the quasi-CW light and the pulses causes diffusion of the pulse position which redetermines the

quasi-CW power profile in the cavity. This diffusion induces a drift velocity of the pulses, similar to a Brownian motion in an inhomogeneous environment that depends on the particles' position.

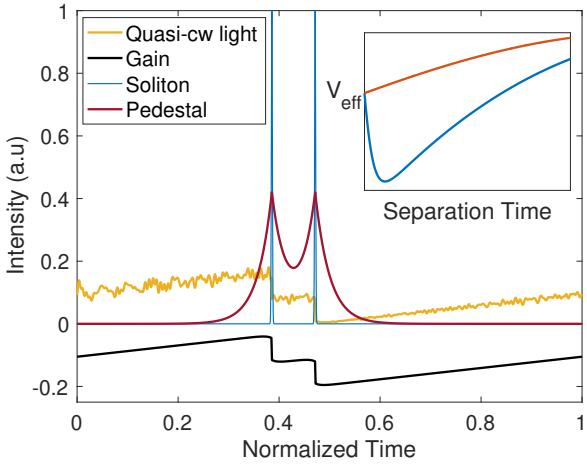

Figure 3: **Illustration of the NMI mechanism.** Passage of soliton pulses through the gain medium depletes the instantaneous gain. A pair of pulses yields a smoothed saw-tooth gain profile. The quasi-CW light light that runs in the cavity is determined by the gain profile, and thus also exhibits a smoothed saw-tooth profile. The NMI is a by-product of the pulse timing jitter caused by nonlinear interaction between the pulses and the quasi-CW light. The inset shows the effective potential for the noise-mediated interaction of the loosely bound (blue) and tightly bound (red) states.

The diffusion constant D_n of the nth pulse is proportional to the local intensity of the quasi-CW, in turn determined by the local net gain as:

$$D_n \propto \left(\frac{1}{\sqrt{l-g_n^-}}+\frac{1}{\sqrt{l-g_n^+}}\right) \tag{2}$$

where l is the total small signal loss and g_n^-, g_n^+ are the gain coefficients before and after the nth pulse, respectively. The variations in g are small compared with the mean gain $\hat{g}$, but may induce large changes in the net loss. Denoting the temporal location of the nth pulse by t_n, its diffusion constant by D_n, and the propagation axis by z, then:

$$\frac{\partial\langle t_n\rangle}{\partial z}=\frac{1}{2}\frac{\partial D_n}{\partial t_n} \tag{3}$$

where the brackets indicate noise-averaging.

Analyzing the drift equation, we find an effective two-pulse potential that determines the steady states. The steady states separation time, governed by the potential minimum, increases with the pedestal energy. The minimum of the effective potential, calculated assuming $\tilde{w} \ll 1$, leads to a stable separation time of [33]:

$$\tilde{t}_s = \tilde{w}\ln\left(\frac{\tilde{E}_{ped}}{\tilde{w}}\right) \tag{4}$$

where $\tilde{t}_s$ is the stable separation time normalized by the cavity round trip time.

In the case where $\tilde{E}_{ped} < \tilde{w}$, the minimum of the potential appears at zero separation time (inset of Figure 3) such that the noise-mediated interaction causes attraction at all separations.

Since the coherent interaction decreases exponentially with the separation time $\tilde{t}_s$, if $\tilde{t}_s >> 1$ the NMI will be the dominant interaction mechanism. However, at smaller separation times, the coherent interaction may be dominant. Therefore, there is a threshold for a phase transition between the NMI induced steady state, i.e loosely bound states, and the coherent interaction induced steady state, i.e tightly bound states. This phase transition, found empirically at $\tilde{t}_s = 0.5\cdot10^{-3}$, is 35 times longer than the pulse duration as will be shown in the next section.

2.3 Soliton Steady States Analysis

We begin this section by applying the theory of NMI to explain the steady states of soliton pairs that we observe experimentally. We then present the steady states in a phase-space diagram. The phase diagram allows us to propose an approach to observe the phase transition between loosely and tightly bound steady states by adjusting the pumping current.

We extract from Figure 1(a-b) the measured separation times between the pulses, and the Kelly sidebands energies, which corresponds to the pedestal energy (See supplementary information, section 1). In Figure 4(a) we present the separation time of the soliton pair, normalized by the cavity round trip time, versus the pedestal energy, normalized by the pulse energy. The dots and triangles correspond to data measured at the loosely bound regime (LB), and at the tightly bound regime (TB). Figure 4(a) shows three different datasets obtained by adjusting the polarization controller to modify the SA behavior. The curves in Figure 4(a) correspond to the prediction of our NMI model, showing a good agreement with the experimental results. We assumed pedestal widths of 77ps, 56ps and 46ps (corresponding to normalized values of $0.80\cdot10^{-3}$, $1.10\cdot10^{-3}$, $0.66\cdot10^{-3}$) for the dataset 1 (yellow), dataset 2 (red) and dataset 3 (blue). While we could not measure the pedestal width directly using the oscilloscope, we estimate its lower bound by the measured width of the Lorentzian shaped Kelly sidebends [41]. We obtain 12.2±0.14ps, 9.8ps ±0.3ps, 10.4 ±0.14ps, (corresponding to normalized values of $0.17\cdot10^{-3}$, $0.14\cdot10^{-3}$, $0.15\cdot10^{-3}$) for experiment 1,2,3, respectively. We note we obtain the lower bounds without compensate for the spreading of

the spectrum due to the $50pm$ resolution of the optical spectrum analyzer, hence the actual pedestal width should be closer to the value we found by the fitting.

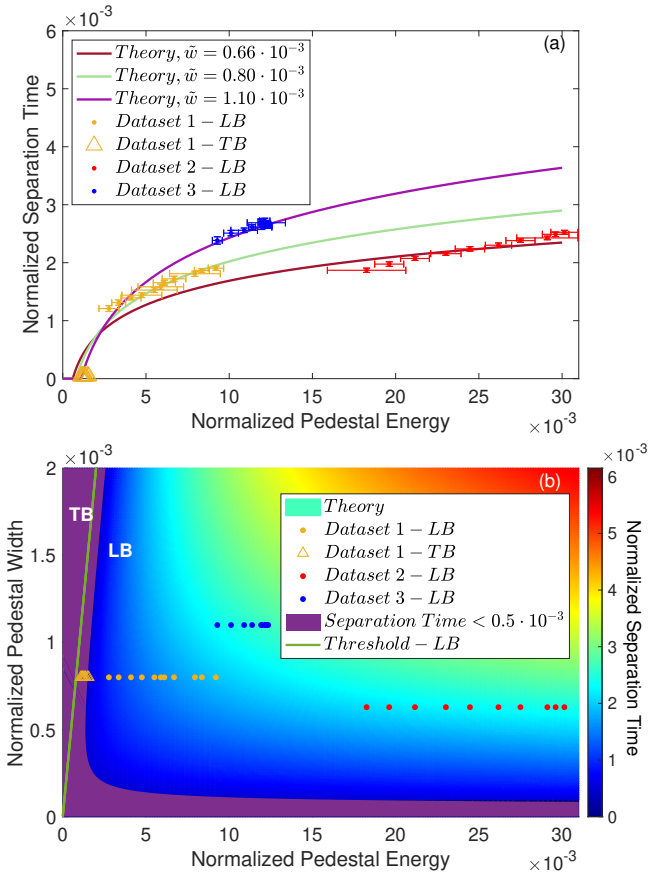

Figure 4: **Soliton steady states analysis.** (a) The measured separation time of the soliton pair, normalized by the cavity round trip time, versus the pedestal energy, normalized by the pulse energy. Three different data sets obtained by adjusting the polarization controller to modify the nonlinear interference in the MMF and thus change the SA properties. The NMI theory (solid line) agrees with the experimental data in the loosely bound (LB) regime and the tightly bound (TB) regime. (b) Theoretically predicted stable separation time for the two pulse loosely bound state plotted as a function of normalized pedestal width and normalized pedestal energy. The yellow line indicates the threshold for a loosely bound state at a non-zero separation time. The purple shaded area marks separation times smaller then $0.5 \cdot 10^{-3}$ in scale of the soliton duration, the NMI is weak comparing to the coherent interaction. Therefore, a phase transition is occur between loosely and tightly bound states. The experimental results are marked by dots (loosely bound) and triangles (tightly bound). The pedestal energy and width are normalized by the total pulse energy, and the cavity round trip time respectively. The dots correspond to the measured steady states presented in panel (a).

We further propose an approach to observe the phase transition between loosely and tightly bound steady states by adjusting the pumping current. By decreasing the pumping current, we decrease the normalized pedestal energy (see supplementary information Figure 2(a) for more details). According to Equation 4, by deceasing the pedestal energy, we continuously decrease the separation time.

By decreasing the pumping current, two scenarios may occur. The first scenario is that the separation time decreases down to the scale of the soliton duration. In this scenario, a phase transition occurs and the separation is locked by the coherent interaction, as explained in the last section. This phase transition occurs between loosely and tightly bound states, presented in the dataset 1 in Figure 4 (b). Note that we observe the transition by tuning only the pumping current and without any external modulation.

The second scenario that may occur when decreasing the pumping current is that the soliton pair state in the cavity become unstable before we reach the threshold for the transition between the loosely and tightly bound states. This case is presented in datasets 2 and 3 in Figure 4 (b). The phase transition can not be observed by reducing the pumping current since the annihilation of one of the soliton occurs before the solitons are close enough to bound coherently.

To achieve these two scenarios in our cavity, we adjust the polarization controller to get different pedestal energies. Our saturable absorber properties, such as linear loss, saturation energy and transission modulation, are unicly sensitive to the polarization. These properties determine the ratio between the pedestal energy and the soliton energy. Therefore by adjusting the polarization controller we can observe both scenarios in the cavity. In practice, in most cases we observe the second scenario while only for extremely low pedestal energies, we observe the first scenario.

3 Conclusions

We experimentally observe and manipulate soliton steady states experimentally and model them with the noise-mediated interaction mechanism. We present a theoretical steady states phase diagram in which we map the areas of parameter space for the tightly and loosely bound states. For the loosely bound states, we calculate the stable separation time and obtain good agreement with the experimental results.

We introduce an approach to control the phase transition between loosely and tightly bound states by decreasing the pedestal energy, utilizing the pumping current with no additional modulators. We also present the ability to avoid this transition by a different configuration of the polarization controller.

We note that the NMI theory predicts the phase tran-

sition independently by reducing the pedestal energy or increasing its width, rather then the pumping current. Instead, an inline spectral filter could lead to the same effect on the pedestal energy to control the steady states. The obtained quantitative agreement with the experiment paves the way to the understanding of complex multi-solitons structures and their control.

References

[1] H-G Purwins, HU Bödeker, and Sh Amiranashvili. Dissipative solitons. *Advances in Physics*, 59(5):485–701, 2010.

[2] Neil Akhmediev and Adrian Ankiewicz. Dissipative solitons in the complex ginzburg-landau and swift-hohenberg equations. In *Dissipative solitons*, pages 1–17. Springer, 2005.

[3] Andreas Liehr. *Dissipative solitons in reaction diffusion systems*. Springer, 2013.

[4] Philippe Grelu and Nail Akhmediev. Dissipative solitons for mode-locked lasers. *Nature photonics*, 6(2):84–92, 2012.

[5] Philippe Grelu. *Nonlinear optical cavity dynamics: from microresonators to fiber lasers*. John Wiley & Sons, 2015.

[6] Yufeng Song, Xujie Shi, Chengfa Wu, Dingyuan Tang, and Han Zhang. Recent progress of study on optical solitons in fiber lasers. *Applied Physics Reviews*, 6(2):021313, 2019.

[7] J Javaloyes, P Camelin, M Marconi, and M Giudici. Dynamics of localized structures in systems with broken parity symmetry. *Physical review letters*, 116(13):133901, 2016.

[8] Piotr Ryczkowski, M Närhi, Cyril Billet, J-M Merolla, Goëry Genty, and John Michaël Dudley. Real-time full-field characterization of transient dissipative soliton dynamics in a mode-locked laser. *Nature Photonics*, 12(4):221–227, 2018.

[9] Xueming Liu and Meng Pang. Revealing the buildup dynamics of harmonic mode-locking states in ultrafast lasers. *Laser & Photonics Reviews*, 13(9):1800333, 2019.

[10] Xueming Liu, Daniel Popa, and Nail Akhmediev. Revealing the transition dynamics from q switching to mode locking in a soliton laser. *Physical review letters*, 123(9):093901, 2019.

[11] Junsong Peng and Heping Zeng. Soliton collision induced explosions in a mode-locked fibre laser. *Communications Physics*, 2(1):1–8, 2019.

[12] Qiu-Yi Ning, Hao Liu, Xu-Wu Zheng, Wei Yu, Ai-Ping Luo, Xu-Guang Huang, Zhi-Chao Luo, Wen-Cheng Xu, Shan-Hui Xu, and Zhong-Min Yang. Vector nature of multi-soliton patterns in a passively mode-locked figure-eight fiber laser. *Optics express*, 22(10):11900–11911, 2014.

[13] Zhenhong Wang, Zhi Wang, Yange Liu, Ruijing He, Jian Zhao, Guangdou Wang, and Guang Yang. Self-organized compound pattern and pulsation of dissipative solitons in a passively mode-locked fiber laser. *Optics letters*, 43(3):478–481, 2018.

[14] Mathias Marconi, Julien Javaloyes, Salvador Balle, and Massimo Giudici. How lasing localized structures evolve out of passive mode locking. *Physical review letters*, 112(22):223901, 2014.

[15] D. J. Richardson, R. I. Laming, D. N. Payne, M. W. Phillips, and V. J. Matsas. 320 fs soliton generation with passively mode-locked erbium fibre laser. *Electronics Letters*, 27(9):730–732, April 1991.

[16] A. B. Grudinin, D. J. Richardson, and D. N. Payne. Passive harmonic modelocking of a fibre soliton ring laser. *Electronics Letters*, 29(21):1860–1861, October 1993.

[17] AN Pilipetskii, EA Golovchenko, and CR Menyuk. Acoustic effect in passively mode-locked fiber ring lasers. *Optics letters*, 20(8):907–909, 1995.

[18] AB Grudinin and S Gray. Passive harmonic mode locking in soliton fiber lasers. *JOSA B*, 14(1):144–154, 1997.

[19] J Nathan Kutz, BC Collings, K Bergman, and WH Knox. Stabilized pulse spacing in soliton lasers due to gain depletion and recovery. *IEEE journal of quantum electronics*, 34(9):1749–1757, 1998.

[20] D. Y. Tang, B. Zhao, D. Y. Shen, C. Lu, W. S. Man, and H. Y. Tam. Compound pulse solitons in a fiber ring laser. *Physical Review A*, 68(1):013816, July 2003.

[21] DY Tang, B Zhao, LM Zhao, and Hwa Yaw Tam. Soliton interaction in a fiber ring laser. *Physical Review E*, 72(1):016616, 2005.

[22] Veronika Tsatourian, Sergey V Sergeyev, Chengbo Mou, Alex Rozhin, Vitaly Mikhailov, Bryan Rabin, Paul S Westbrook, and Sergei K Turitsyn. Polarisation dynamics of vector soliton molecules in mode locked fibre laser. *Scientific reports*, 3(1):1–8, 2013.

[23] ZQ Wang, K Nithyanandan, A Coillet, P Tchofo-Dinda, and Ph Grelu. Optical soliton molecular complexes in a passively mode-locked fibre laser. *Nature communications*, 10(1):1–11, 2019.

[24] Andrey Komarov, Konstantin Komarov, and François Sanchez. Quantization of binding energy of structural solitons in passive mode-locked fiber lasers. *Physical Review A*, 79(3):033807, 2009.

[25] LM Zhao, DY Tang, Han Zhang, and X Wu. Bunch of restless vector solitons in a fiber laser with sesam. *Optics express*, 17(10):8103–8108, 2009.

[26] YF Song, H Zhang, LM Zhao, DY Shen, and DY Tang. Coexistence and interaction of vector and bound vector solitons in a dispersion-managed fiber laser mode locked by graphene. *Optics express*, 24(2):1814–1822, 2016.

[27] Chong Wang, Lu Wang, Xiaohui Li, Wenfeng Luo, Tianci Feng, Ying Zhang, Penglai Guo, and Yanqi Ge. Few-layer bismuthene for femtosecond soliton molecules generation in er-doped fiber laser. *Nanotechnology*, 30(2):025204, 2018.

[28] Chengbo Mou, Sergey V Sergeyev, Aleksey G Rozhin, and Sergei K Turitsyn. Bound state vector solitons with locked and precessing states of polarization. *Optics express*, 21(22):26868–26875, 2013.

[29] NN Akhmediev, A Ankiewicz, and JM Soto-Crespo. Stable soliton pairs in optical transmission lines and fiber lasers. *JOSA B*, 15(2):515–523, 1998.

[30] Ph Grelu, F Belhache, F Gutty, and J-M Soto-Crespo. Phase-locked soliton pairs in a stretched-pulse fiber laser. *Optics letters*, 27(11):966–968, 2002.

[31] MJ Lederer, Barry Luther-Davies, HH Tan, C Jagadish, NN Akhmediev, and JM Soto-Crespo. Multipulse operation of a ti: sapphire laser mode locked by an ion-implanted semiconductor saturable-absorber mirror. *JOSA B*, 16(6):895–904, 1999.

[32] Michel Olivier and Michel Piché. Origin of the bound states of pulses in the stretched-pulse fiber laser. *Optics express*, 17(2):405–418, 2009.

[33] Rafi Weill, Alexander Bekker, Vladimir Smulakovsky, Baruch Fischer, and Omri Gat. Noise-mediated casimir-like pulse interaction mechanism in lasers. *Optica*, 3(2):189–192, 2016.

[34] Jae K Jang, Miro Erkintalo, Stuart G Murdoch, and Stéphane Coen. Ultraweak long-range interactions of solitons observed over astronomical distances. *Nature Photonics*, 7(8):657–663, 2013.

[35] Wenbin He, Meng Pang, Dung-Han Yeh, Jiapeng Huang, CR Menyuk, and P St J Russell. Formation of optical supramolecular structures in a fibre laser by tailoring long-range soliton interactions. *Nature communications*, 10(1):1–9, 2019.

[36] Jose M Soto-Crespo, Nail Akhmediev, Ph Grelu, and F Belhache. Quantized separations of phase-locked soliton pairs in fiber lasers. *Optics letters*, 28(19):1757–1759, 2003.

[37] Yi Zhou, Yu-Xuan Ren, Jiawei Shi, Huade Mao, and Kenneth KY Wong. Buildup and dissociation dynamics of dissipative optical soliton molecules. *Optica*, 7(8):965–972, 2020.

[38] Luca Nimmesgern, Cornelius Beckh, Hannes Kempf, Alfred Leitenstorfer, and Georg Herink. Soliton molecules in femtosecond fiber lasers: universal binding mechanism and direct electronic control. *Optica*, 8(10):1334–1339, 2021.

[39] Kfir Sulimany, Ohad Lib, Gilad Masri, Avi Klein, Moti Fridman, Philippe Grelu, Omri Gat, and Hadar Steinberg. Bidirectional soliton rain dynamics induced by casimir-like interactions in a graphene mode-locked fiber laser. *Physical review letters*, 121(13):133902, 2018.

[40] Hendrik BG Casimir and Dirk Polder. The influence of retardation on the london-van der waals forces. *Physical Review*, 73(4):360, 1948.

[41] Rafi Weill, Alexander Bekker, Vladimir Smulakovsky, Baruch Fischer, and Omri Gat. Spectral sidebands and multipulse formation in passively mode-locked lasers. *Physical Review A*, 83(4):043831, 2011.

[42] Elham Nazemosadat and Arash Mafi. Nonlinear multimodal interference and saturable absorption using a short graded-index multimode optical fiber. *JOSA B*, 30(5):1357–1367, 2013.

[43] Fengyan Zhao, Hushan Wang, Yishan Wang, Xiaohong Hu, Ting Zhang, and Ran Pan. Observation of various bound states based on a graded index multimode fiber saturable absorber. *Laser Physics Letters*, 17(2):025105, 2020.

[44] Shijie Fu, Quan Sheng, Xiushan Zhu, Wei Shi, Jianquan Yao, Guannan Shi, Robert A Norwood, and N Peyghambarian. Passive q-switching of an all-fiber laser induced by the kerr effect of multimode interference. *Optics express*, 23(13):17255–17262, 2015.

[45] Huanhuan Li, Zhaokun Wang, Can Li, Junjie Zhang, and Shiqing Xu. Mode-locked tm fiber laser using smf-simf-gimf-smf fiber structure as a saturable absorber. *Optics express*, 25(22):26546–26553, 2017.

[46] Zhaokun Wang, DN Wang, Fan Yang, Liujiang Li, Chunliu Zhao, Ben Xu, Shangzhong Jin, Shiying Cao, and Zhanjun Fang. Er-doped mode-locked fiber laser with a hybrid structure of a

step-index–graded-index multimode fiber as the saturable absorber. *Journal of Lightwave Technology*, 35(24):5280–5285, 2017.

[47] Zhaokun Wang, DN Wang, Fan Yang, Liujiang Li, Chun-Liu Zhao, Ben Xu, Shangzhong Jin, Shi-Ying Cao, and Zhan-Jun Fang. Stretched graded-index multimode optical fiber as a saturable absorber for erbium-doped fiber laser mode locking. *Optics letters*, 43(9):2078–2081, 2018.

[48] Uğur Teğin and Bülend Ortaç. All-fiber all-normal-dispersion femtosecond laser with a nonlinear multimodal interference-based saturable absorber. *Optics letters*, 43(7):1611–1614, 2018.

[49] Fan Yang, DN Wang, Zhaokun Wang, Liujiang Li, Chun-Liu Zhao, Ben Xu, Shangzhong Jin, Shi-Ying Cao, and Zhan-Jun Fang. Saturable absorber based on a single mode fiber–graded index fiber–single mode fiber structure with inner micro-cavity. *Optics express*, 26(2):927–934, 2018.

[50] Tao Chen, Qiaoli Zhang, Yaping Zhang, Xin Li, Haikun Zhang, and Wei Xia. All-fiber passively mode-locked laser using nonlinear multimode interference of step-index multimode fiber. *Photonics Research*, 6(11):1033–1039, 2018.

[51] Fengyan Zhao, Ning Li, and Hushan Wang. Generation of a noise-like pulse from an erbium-doped fiber laser based on nonlinear multimode interference. *Laser Physics*, 30(12):125102, 2020.

[52] Fengyan Zhao, Hushan Wang, Xiaohong Hu, Yishan Wang, Wei Zhang, Ting Zhang, Chuandong Sun, and Zhijun Yan. Experimental observation of bound solitons with a nonlinear multimode interference-based saturable absorber. *Laser Physics Letters*, 15(11):115106, 2018.

[53] SMJ Kelly. Characteristic sideband instability of periodically amplified average soliton. *Electronics Letters*, 28(8):806–807, 1992.

[54] J. P. Gordon. Dispersive perturbations of solitons of the nonlinear Schrödinger equation. *Journal of the Optical Society of America B*, 9(1):91, January 1992.

[55] A.B. Grudinin, D.J. Richardson, and D.N. Payne. Energy quantisation in figure eight fibre laser. *Electronics Letters*, 28(1):67–68, January 1992.

[56] D. Y. Tang, L. M. Zhao, B. Zhao, and A. Q. Liu. Mechanism of multisoliton formation and soliton energy quantization in passively mode-locked fiber lasers. *Phys. Rev. A*, 72(4):043816, 2005.

[57] Rafi Weill, Boris Vodonos, Ariel Gordon, Omri Gat, and Baruch Fischer. Statistical light-mode dynamics of multipulse passive mode locking. *Physical Review E*, 76(3):031112, September 2007.

[58] H.A. Haus and A. Mecozzi. Noise of mode-locked lasers. *IEEE Journal of Quantum Electronics*, 29(3):983–996, March 1993.

[59] Michael Katz, Omri Gat, and Baruch Fischer. Noise-induced oscillations in fluctuations of passively mode-locked pulses. *Optics Letters*, 35(3):297–299, February 2010.